








# Silicate bonding of sapphire to SESAMs: adjustable thermal lensing for high-power lasers

L. LANG,<sup>1,3,\*</sup>  F. SALTARELLI,<sup>1,3</sup>  G. LACAILLE,<sup>2</sup> S. ROWAN,<sup>2</sup> J. HOUGH,<sup>2</sup> I. J. GRAUMANN,<sup>1</sup>  C. R. PHILLIPS,<sup>1</sup>  AND U. KELLER<sup>1</sup> 

<sup>1</sup>*Institute for Quantum Electronics, ETH Zurich, 8093 Zurich, Switzerland*

<sup>2</sup>*Institute for Gravitational Research, University of Glasgow, G12 8QQ Glasgow, UK*

<sup>3</sup>*These authors contributed equally to this work*

\*[langl@phys.ethz.ch](mailto:langl@phys.ethz.ch)

**Abstract:** Silicate bonding is a flexible bonding method that enables room-temperature bonding of many types of materials with only moderate flatness constraints. It is a promising approach for bonding components in high power laser systems, since it results in a thin and low-absorption interface layer between the bonded materials. Here we demonstrate for the first time silicate bonding of a sapphire window to a Semiconductor Saturable Absorber Mirror (SESAM) and use the composite structure to mode-lock a high-power thin-disk laser. We characterize the fabricated devices both theoretically and experimentally and show how the thermally induced lens of the composite structure can be tuned both in magnitude and sign via the thickness of the sapphire window. We demonstrate mode-locking of a high-power thin-disk laser oscillator with these devices. The altered thermal lens allows us to increase the output power to 233 W, a 70-W-improvement compared to the results achieved with a state-of-the-art SESAM in the same cavity.

Published by The Optical Society under the terms of the [Creative Commons Attribution 4.0 License](https://creativecommons.org/licenses/by/4.0/). Further distribution of this work must maintain attribution to the author(s) and the published article's title, journal citation, and DOI.

## 1. Introduction

High-power ultrafast laser sources find many applications in research and industry. The high peak powers are useful for industrial micro-machining or generation of extreme-ultra-violet and terahertz radiation, and the ultrashort pulses enable time resolution down to the femtosecond timescale. Currently, the leading technologies for high power ultrafast lasers use Yb-doped gain media based on thin-disk, innoslab and fiber configurations [1–4]. All three configurations are routinely used to generate multi-100-W average output powers, owing to the excellent thermal characteristics and geometry of the gain material. In a thin-disk laser (TDL), the gain is disk-shaped with order 100- $\mu\text{m}$  thickness and is used in reflection, with the back-side being attached to a water-cooled heat-sink. This enables a quasi-one-dimensional heat-flow which results in highly efficient heat extraction. Consequently, the TDL technology enables the generation of a high-power laser output directly from an oscillator [1]. Such oscillators are very attractive due to their lower complexity compared with laser amplifier systems. Ultrafast operation in TDLs is typically achieved using either Semiconductor Saturable Absorber Mirror (SESAM) mode-locking [5] or Kerr-Lens Mode-locking (KLM), which have achieved 350 W [1] and 270 W [6] average output powers, respectively.

Managing the thermal load on the intracavity components is one of the major challenges in power-scaling these lasers [7]. Heating of components typically leads to thermal lensing effects, changing the cavity mode and ultimately limiting performance. In particular, the absorptive nature of the SESAM leads to a non-negligible heat load and thermal lens on the structure. One

possible solution to mitigate this effect is the use of adaptive optics like deformable mirrors to compensate for the thermal lensing of the intracavity components [8]. While this solution enabled more than 1 kW of continuous-wave (cw) output power in a TDL, it increases the complexity of the laser system and has not yet been demonstrated in a high-power mode-locked laser. Many strategies to more directly combat SESAM thermal lensing have also been explored, such as thinner substrates, improved contacting [1], or substrate transfer followed by etching [9]. The substrate transfer technique led to exceptionally flat surfaces (ROC > 1 km) and outstanding heat extraction. However, due to growth related defects and asymmetries in our MBE machine, we were not able to obtain a large area sample with such bonding, which would be needed for a high-power TDL. As an alternative without the inherent thermal lens of the SESAM, nonlinear mirror mode-locking has also been employed to mode-lock thin-disk lasers [10,11]. So far, however, mode-locking instabilities prevented the use of this technique above 100-W average power.

Here we demonstrate a new approach based on silicate bonding a sapphire window to the front-face of a SESAM. This bonding process was developed for research in astronomy and gravitational wave detection [12], and has since been applied to various materials including sapphire [13]. The optical properties of the bond have recently gathered increasing interest to expand the range of applications to the field of photonics [14]. In fact, silicate bonding has a unique combination of properties that make it a promising candidate for the fabrication of devices for high-power or ultrafast lasers: First, the bond is optically clear and has a high damage threshold. The bond can therefore be used for intra-cavity bonds in high-power lasers, as we demonstrate here. Second, the bonding process does not require atomically flat surfaces. In fact, we apply it successfully to bond standard optical quality sapphire windows to as-grown SESAMs that show strain induced defects and bending. And third, the bonding process works at room temperature. This property makes it compatible with devices such as SESAMs whose properties change when annealed at high temperatures.

In this work, we demonstrate silicate bonding of sapphire to a SESAM for the first time, to the best of our knowledge. The fabricated device is used in a high-power TDL, leading to a significant increase in output power. In a first step, we bond sapphire windows of several thicknesses to SESAMs. We then characterize the thermal lens of the fabricated devices and implement a 3D thermo-optic simulation to model the expected behavior. The model shows how the sign and magnitude of the SESAM thermal lens can be tuned by varying the thickness of the sapphire. We find good agreement between the experimental results and theoretical predictions. Finally, we use the new SESAMs to mode-lock a high-power 1030-nm TDL and achieve 233-W average power, 734-fs pulse duration at 10.2-MHz repetition rate. In the same cavity, we also tested a conventional high-power SESAM of the type used in our recent high-power results [1], and obtained up to 160 W mode-locked power. Hence, the sapphire-bonded SESAM enabled a 70-W improvement in this case. We show how this improvement can be attributed to a change in sign of the thermal lens of the SESAM.

Our solution enables high-power compatible mirrors with adjustable thermal properties fabricated by a versatile and convenient room-temperature bonding technique. In addition to the SESAM devices we demonstrate in this work, our approach is applicable to a wide range of reflective optics, including for example vertical external cavity surface emitting lasers (VECSELs).

## 2. Silicate bonding

Silicate bonding uses a hydroxide solution to catalyze the formation of a silica-based network between two surfaces, effectively bonding them together. The technique was initially developed for structural applications in instruments for astronomy and became one of the main contributors to the multiple breakthroughs in gravitational wave detections in the past few years [12,15,16].

Although not as impactful in photonics, its set of properties have pulled interest from the field and works on characterization of the optical performances of the bond were carried out [17,18]. It provides advantageous features when compared to the main techniques used in the industry, adhesive bonding and direct bonding. Other room temperature processes that have been developed for photonics applications by industrial concerns include Adhesive-Free Bonding (AFB) or Chemically Activated Direct Bonding (CADB) [19,20].

Adhesive bonds can display a large range of properties due to the flexibility in formulation. The main drawbacks come from their organic nature which make them subject to outgassing and light-induced damage at high power [21,22]. Additionally, there is a large discrepancy between the thermo-mechanical properties of non-specialized optical adhesives and the substrates they are used for. This can lead to reduced mechanical stability and increased thermally induced stress when the component is subject to a change in temperature [21].

Direct bonding, at low or elevated temperature, constitutes the state-of-the-art of high-performance bonds for optical applications [23,24]. After a surface activation process, two components with smooth, matching surfaces (or the capacity to deform sufficiently for them to match) are able to bond readily at room temperature with moderate pressure. The interface being free from a third layer, an “ideal” bond is formed with regards to mechanical stability and outgassing. In practice, it is hard to obtain a homogeneous interface due to the stringent requirements on the surface quality. Post processing of the component, e.g. heating at high temperature [23] or applying a voltage across the interface [25], is common to increase the strength of the bond, but cannot be applied to SESAMs as this would cause changes in their saturation properties or even destroy them.

Silicate bonding avoids the issues met with adhesive bonding by only using inorganic components and forming a thin, glass-like bond which guarantees good mechanical stability and structural integrity for a wide range of temperatures [26,27]. Compared to direct bonding techniques, silicate bonding gives some leniency on the surface quality requirements thanks to the use of a solution which can make up for small surface mismatch between the parts. It also has the advantage to be a cheap and easy-to-implement room temperature process. A potential drawback is the insertion of a silica layer in the system that can produce unwanted reflections at the interface [17,18]. However, we have confirmed this not to be an issue for the devices fabricated in this work.

According to the original patent, the technique can be used to bond both gallium-arsenide (GaAs) and sapphire [27]. To the best of our knowledge, there is no available report on GaAs bonding, whereas sapphire has already been the focus of several works including in hybrid bonds with silicon [13,28]. It is understood that bonding works by etching the surface of the sapphire to develop an aluminosilicate network as described in [29]. The hypothesis is that a similar reaction happens at the surface of the SESAM to form Ga-O and As-O bonds for the network to hang on to, although more investigation is needed on the exact chemistry happening.

### **3. Device fabrication, characterization and modeling**

#### *3.1. Fabrication*

The fabrication process of the sapphire bonded SESAMs is shown in Fig. 1. The SESAMs were designed in-house and fabricated in the FIRST cleanroom facilities of ETH Zurich. The design is based on previous designs from our group [1] and includes three quantum wells in a single antinode as saturable absorbers. Compared to standard SESAMs, the sapphire window will lead to a threefold increase of the fluence inside the SESAM structure due to a reduction of the index-mismatch of the air-semiconductor interface. We include 1–2 additional layer pairs on top of the absorber section to counteract this and reduce the fluence in the quantum wells. After growth (Fig. 1(a)), the samples were bonded to sapphire windows using a standard procedure for silicate bonding as described in e.g. [13]. The sapphire windows are c-cut to reduce birefringence,

and have a  $0.5^\circ$  wedge to prevent mode-locking instabilities caused by the residual reflection from the front surface. The bonding solution is prepared by diluting a commercial aqueous sodium silicate solution (Sigma Aldrich 338443) containing approximately 11% sodium hydroxide and 27% silicate in weight in deionized water to a volumetric ratio of 1 to 6. The solution is then centrifuged to segregate the larger particles and pressed through 200 nm medical filters to remove the smaller ones.

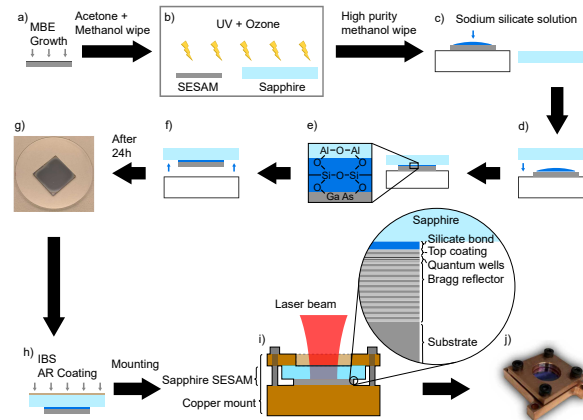


**Fig. 1.** Fabrication of a sapphire SESAM. a) Molecular-beam epitaxy (MBE) growth of the SESAM epitaxial structure. b) The SESAM and a sapphire window are exposed to UV radiation (185 and/or 254 nm) and ozone for a total of 26 min. c) The sodium silicate solution is put in a single drop at the center of the SESAM after a final wipe with high purity methanol. d) The sapphire window is brought into contact gently with no other pressure than its self-weight and the solution spreads between the two parts. e) The solution slightly etches the surfaces and upon dehydration forms a dense, cross-linked network of silica. f) After about 5 minutes, the sample can be lifted and moved to cure further before being tested. g) After 24 hours, the bond appears homogeneous over the optical aperture of the sample. h) An anti-reflective coating is applied to the sapphire window via ion beam sputtering (IBS). i) The SESAM is mounted in a copper cooling mount. The inset shows the full layer structure of the fabricated sapphire SESAM. j) Picture of the complete device.

The surfaces are made hydrophilic using UV/Ozone cleaning in a custom-built enclosure. This differs from the usual cerium oxide scrubbing procedure as the SESAMs cannot tolerate it. UV/Ozone cleaning uses 185-nm and 254-nm light to generate oxygen radicals that react with organic species adsorbed on the surfaces and turns them into gas that desorb in the atmosphere [30]. The resulting surfaces have the cleanliness required for successful bonding.

The surfaces are first cleaned with reagent grade acetone and methanol. The samples are then placed in the cleaning enclosure, and the low-pressure mercury bulbs are started (Fig. 1(b)). For the first 11 minutes, both wavelengths are produced to fill the box with ozone (up to 200 ppm) and catalyze the reaction with the contaminants. Then the 185-nm light is turned off and the ozone is degraded under the action of 254-nm radiation for an additional 15 min before the box is safe to be opened again. The samples are then taken to be bonded on a laminar flow bench. The SESAM is placed on a Teflon support to prevent unwanted bonding should there be any overspill of bonding solution. A final wipe of the surfaces with high purity methanol (Chromasolv for High Performance Liquid Chromatography) is carried out. A volume of solution amounting to  $0.8 \mu\text{l}/\text{cm}^2$  of bonding area is drawn up with a micropipette and laid on the surface of the SESAM in a single drop (Fig. 1(c)). The sapphire window is slowly brought into contact to allow the solution to spread without trapping air bubbles (Fig. 1(d)). The SESAM is maintained roughly at

the center by touching the edge of the window but with no added pressure. A 3-dimensional silica network develops through etching, polymerization and dehydration (Fig. 1(e)). After a few minutes, the bond forms with a strength sufficient for the sample to be moved (Fig. 1(f)). A photograph of one of the bonded samples is shown in Fig. 1(g).

Sixteen samples were bonded this way using varying thickness of sapphire windows (0.2, 0.3, 0.5 and 3.0 mm). All samples were observed to bond well within a few minutes. The samples were left to cure in ambient atmosphere for ten days. The sapphire windows were then coated with an anti-reflective coating (University of Neuchatel) optimized for 632 nm (<1% reflectivity) and 1000–1100 nm (<0.02% reflectivity) to facilitate the interferometer measurements and reduce losses in the laser, respectively (Fig. 1(h)). Finally, the samples are mounted in a copper mount built in-house (Fig. 1(i)). First, some thermal paste is applied to a copper heatsink and the SESAM placed onto it. A copper front-plate is then screwed on to hold the SESAM in place while applying only little pressure. A photograph of a fully assembled and mounted sapphire SESAM is shown in Fig. 1(j).

### 3.2. Characterization and modeling

We characterize the power dependent thermal lens of the fabricated devices using an interferometer based setup as previously shown in [9]. The setup (Fig. 2(a)) uses a high-power cw thin-disk laser source delivering up to 180 W at 1030 nm to induce a high thermal load on the SESAM. The laser is attenuated with a half-wave plate and thin-film polarizer to allow the power incident on the sample to be continuously tuned. A lens is used to set the laser spot size on the sample to  $800 \mu\text{m } 1/e^2$  radius. We measure the curvature of the sample through a 2" 45° mirror close to the sample using a Twyman-Green interferometer (TRIOPTICS  $\mu$ Phase 500). Compared to [9], we insert a 4f-imaging setup to image the sample onto the image plane of the interferometer. This ensures high accuracy of the recorded curvatures over a broad range of sample curvatures. The camera placed behind the same 2" 45° mirror is used to measure the laser spot size at the sample position.

For each sample, we record the surface profile for incident powers in the range 0–160 W (exemplary measurement shown in Fig. 2(b)). We extract the effective lens in a circle with 1.6 mm radius centered on the laser beam. We then compute the change in thermal lens as a function of absorbed power, i.e.  $dF_{\text{th}}/dP_{\text{abs}}$ , and plot it versus sapphire thickness in Fig. 2(c). We also determine the astigmatism of the lens by computing the difference along the two major axes of the parabolic part of the lens, and find that the sapphire samples on average have 50% less astigmatism compared to standard SESAMs. The results show that the sign of the thermal lens is flipped compared to standard SESAMs (0 mm sapphire), and how the strength of the thermal lens can be tuned by adjusting the thickness of the sapphire window. We note that the thermal lensing of the standard SESAMs with no sapphire varies significantly between the samples. We attribute this to the different contacting techniques used, which has previously been shown to strongly impact the lensing [9].

To better understand the thermo-optic properties of these devices we have implemented a finite element model in COMSOL to simulate the thermal lensing. The model (output schematically shown in Fig. 2(d)) accounts for both the lensing due to thermal expansion and the lensing due to the thermo-optic coefficient  $dn/dT$  of the sapphire window. The device is modeled as consisting of the following layers: A copper heatsink with a fixed temperature, a soft thermal interface material, a gallium-arsenide (GaAs) substrate, a Bragg reflector, a quantum-well (QW) absorber section, some additional Bragg-reflector layers, the silicate bond, the sapphire window, and finally another copper heatsink on the sides. We account for the reduced thermal conductivity of the thin-film structure based on [31]. The interface material between the copper heatsink and the SESAM is assumed to be soft to model the thermal paste used for the sapphire SESAMs. Since the stiffness of this layer has been observed to have little impact on the results, we use



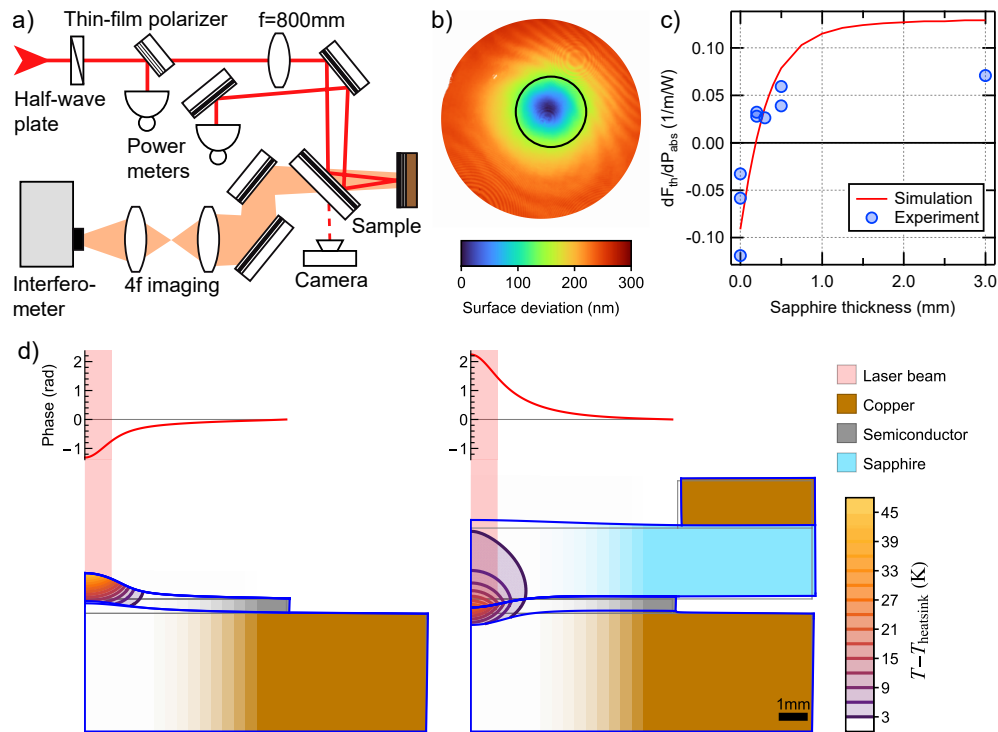


**Fig. 2.** a) The setup used to measure the thermal lens of the SESAMs as a function of incident power. The cw laser beam is attenuated with a half-wave plate and thin-film polarizer, and focused onto the sample using a lens. The sample surface is measured through a 2" mirror close to the sample using an interferometer. b) Measured deviation from cold for a sapphire SESAM at 160 W incident power. The black circle indicates the 1.6-mm-radius-disk used to compute the local curvature. c) Strength of the thermal lens  $dF_{th}/dP_{abs}$  as a function of sapphire thickness. Experimental data points are measured with our interferometer-based setup and the theoretical curve was computed with our finite element model. d) Schematic of the finite element model showing the deformation assuming 5 W of absorbed power (to make the deformation visible, it is scaled up by  $\times 5000$ ) for a standard SESAM with no sapphire (left) and a SESAM with a 3.0 mm (right) sapphire window bonded on top. The grey and blue lines indicate the outline of the undeformed and deformed structure, respectively. The temperature profile is indicated by the contours and shows that the heat is concentrated in the absorber region of the SESAM. The  $1/e^2$  width of the laser beam is shown in red. The curves at the top show the optical phase picked up by the beam as a function of radial position.

the interface material also for the standard SESAM, which is usually soldered onto the copper heatsink. The heat is assumed to be entirely generated within the QW section with a Gaussian intensity profile.

Figure 2(d) shows the computed deformation (scaled up by  $\times 5000$ ) and temperature profile for 5 W of absorbed power, for the case of no sapphire (left) and a 3.0 mm thick sapphire window (right). These 5 W of absorbed power correspond to the operating point of the SESAM at the highest output power in our high-power mode-locking experiments discussed in the next section. The curves at the top show the optical phase picked up by the laser beam as a function of radial position. As can be seen, a standard SESAM will lead to a defocusing lens due to the thermal expansion of the GaAs substrate. For the sapphire SESAM on the other hand, the resulting lens will be focusing due to two effects: First, the thermal expansion of the sapphire will press the SESAM inwards, and second, the positive thermo-optic coefficient of sapphire leads to an additional focusing lens due to the temperature profile within the window. We repeat the analysis done on the experimental results to extract the slope  $dF_{th}/dP_{abs}$  of the thermal lens for different thicknesses of the sapphire window and plot the result in Fig. 2(c) (solid red line). We see good qualitative agreement between the experimental results and the theoretical predictions in Fig. 2(c). The quantitative agreement is reasonable given the lack of any fitting parameters in the model. The thermal lens is being overestimated by the model however, especially for the SESAM with a 3.0 mm sapphire window. Importantly however, the model correctly predicts that the strength of the thermally induced lens, including its sign, can be tuned by changing the sapphire thickness. It is in principle possible to obtain a SESAM with no overall thermal lensing when choosing the appropriate thickness for the sapphire window. In fact, we achieve approximately a two-fold reduction in thermal lensing for the SESAMs with 0.2 mm and 0.3 mm sapphire windows compared to standard SESAMs soldered to a copper heatsink.

## 4. High-power mode-locked operation

### 4.1. Thin-disk laser cavity

We use the SESAMs in a high-power TDL cavity to verify their suitability for high-power ultrafast operation. The cavity (Fig. 3(a)) is based on previous designs from our group [10]. It incorporates an active multipass cell [32] with three passes on the Yb-doped thin-disk (TRUMPF, see also Fig. 3(b), highlighted gray region), enabling the use of a 30% output coupler to optimize output power. A thin-film polarizer is used to select the polarization. To initiate and stabilize mode-locking, we insert a SESAM as end-mirror. As we rely on soliton mode-locking [33], we balance the self-phase-modulation (SPM) with negative group-delay-dispersion (GDD). The amount of SPM is reduced by partially evacuating the vacuum chamber that contains the laser cavity. To balance the residual SPM picked up by the pulses, four dispersive mirrors with  $2 \times -550\text{fs}^2$  (Layertec) and  $2 \times -2000\text{fs}^2$  (University of Neuchatel) are used, providing a total of  $-30600\text{fs}^2$  GDD per roundtrip. Both types of dispersive mirrors support 100 fs pulses. The cavity reaches up to 220 W output power in cw operation, and up to 160 W in mode-locked operation when using a state-of-the-art SESAM grown in-house and contacted by TRUMPF.

To reach optimal efficiency while maintaining single-mode operation, the size of the cavity mode (Fig. 3(b)) must be scaled to the size of the pump spot on the disk. The ideal ratio is typically reached with the cavity mode being around 70–80% the size of the pump spot depending on the particular cavity and pump profile [34,35]. However, the exact mode size on the disk (see Fig. 3(b), highlighted red points) depends on the thermal lensing of the intracavity components. In Fig. 3(c), we show the dependence of this mode size as a function of the thermal lens on the disk  $\Delta F_{th,disk}$  (solid blue line). As can be seen, the cavity is designed such that it operates around the center of its stability zone with respect to thermal lensing. To illustrate the role of the additional thermal lens of the SESAM, we set its thermal lens to a fixed multiple of  $\Delta F_{th,disk}$ . As shown in Fig. 3(c), the shape of the stability zone depends strongly on the lens ratio

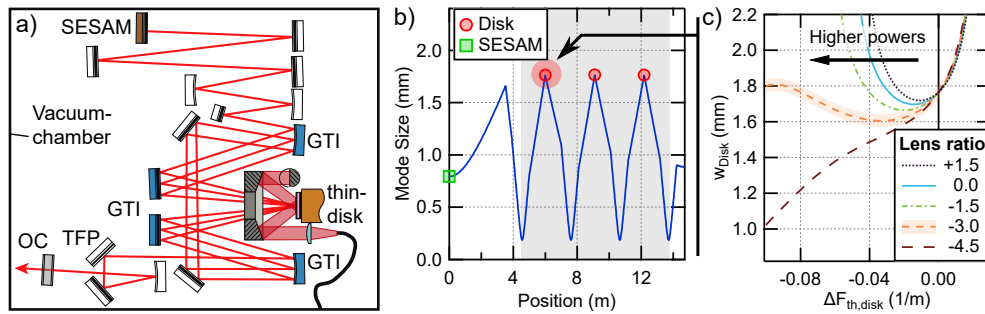


**Fig. 3.** a) The cavity used for the mode-locking experiments. It includes three passes on the thin disk, a thin-film polarizer for polarization control and dispersive mirrors for dispersion control. The cavity is built inside a vacuum chamber to control the air pressure. b) Evolution of the  $1/e^2$  cavity mode radius. The region highlighted in gray indicates the multipass scheme on the disk. The red points indicate the disk. c) The cavity mode size on the disk as a function of the thermal lens on the disk, for several values of the lens ratio  $\Delta F_{th,SESAM}/\Delta F_{th,disk}$ , i.e. the ratio between the SESAM's thermal lens and the disk's thermal lens. The highlighted orange curve indicates a favorable lens ratio leading to a widening of the stability zone.

$\Delta F_{th,SESAM}/\Delta F_{th,disk}$ . For values around  $-3.0$  (highlighted, orange), the thermal lenses partially counteract each other. This in turn leads to a significant widening of the stability zone, extending the range of thermal lenses where there is a suitable spot size in the thin disk.

#### 4.2. High power mode-locked operation

We tested SESAMs with four different thicknesses of sapphire (0.2, 0.3, 0.5 and 3.0 mm) and one standard SESAM without sapphire window. After slightly adjusting the cavity to locate a spot on the SESAM with favorable cold curvature, we achieve stable mode-locking over a wide range of output powers, reaching more than 160 W in all cases. For increasing output powers, the pulse duration decreases as expected for soliton pulse shaping. Hence, to keep the pulse duration within a suitable range for stable mode-locking, we reduce the intra-cavity air pressure to optimize mode-locking stability for higher powers. We verify fundamental mode-locking using the standard mode-locking diagnostics: We record the optical spectrum of the pulses, the auto-correlation trace using a 200-ps long-range autocorrelator, an oscilloscope trace using a 45-GHz sampling oscilloscope, and the micro-wave spectrum of the pulse train. In Fig. 4(a), we show the average output power as a function of pump power both for the standard SESAM (red squares) and for the SESAM with 3.0 mm sapphire (blue circles): We reach a maximum average output power of 233 W using a SESAM with a 3.0 mm sapphire window, which is a 70-W-improvement over the standard SESAM. The mode-locking diagnostics are displayed in Fig. 4(b)–4(e) and show a repetition rate of 10.2 MHz with a pulse duration of 734 fs assuming  $\text{sech}^2$  pulses, corresponding to a time-bandwidth product of  $1.13 \times 0.315$ . The air pressure in the laser cavity was 166 mbar. We attribute the improved output power to the compensation of the thermal lenses of the SESAM and disk. In fact, based on our extra-cavity measurements of the thermal lenses, we estimate the lens ratio to be  $\Delta F_{th,SESAM}/\Delta F_{th,disk} \approx -2.9$ , which is very close to the favorable ratio suggested by Fig. 3(c) (highlighted orange line). This shows that a non-zero thermal lens of the SESAM can in fact lead to a performance improvement if it counteracts the lens of the disk. These results demonstrate the flexibility of the sapphire bonded SESAMs: with an optimal choice of the thickness of the sapphire, a large fraction of the thermal lens of the active medium or other components can be compensated.



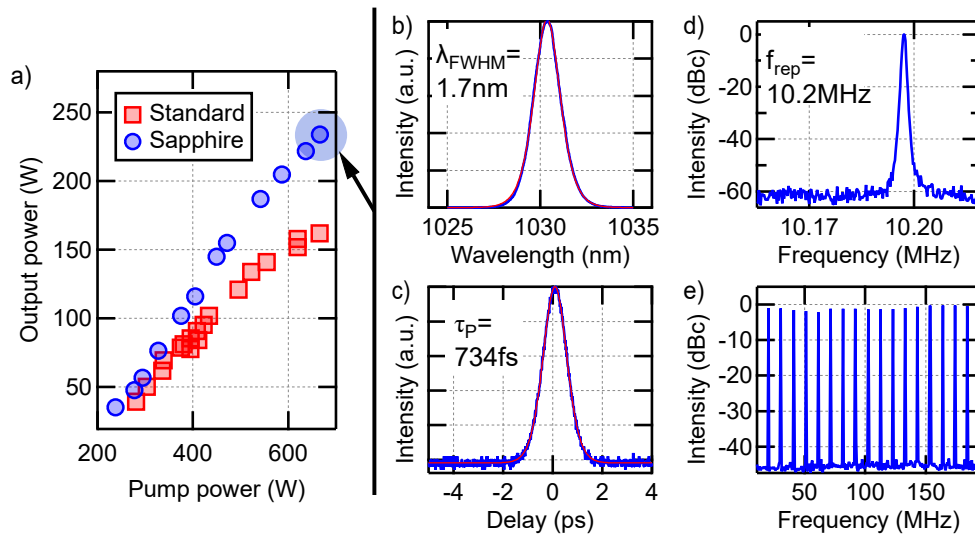


**Fig. 4.** a) The average output power as a function of pump power for a standard SESAM (red squares) and a SESAM with a 3.0-mm sapphire on top (blue circles). b)-e) Mode-locking diagnostics for the highest output power of the sapphire SESAM (highlighted on the left). Shown are the autocorrelation trace (b), optical spectrum of the pulses (c), microwave spectrum of the pulse train around the repetition rate of the cavity (d) and over a broader range (e).

#### 4.3. Outlook on further power scaling

While achieving the high-power results presented here, we have not observed any damage to the silicate bond. Hence, we anticipate significant potential for power scaling using this new SESAM technology. For our record average power TDL oscillator results we used a much larger pump spot size than used here (6 mm instead of 3.6 mm), which enabled scaling up to 350 W [1]. The power achievable in that case appeared to be limited by SESAM thermal lensing which brought the cavity out of the optimal laser-to-pump spot size ratio. Hence, our results here represent a very promising path to further power scaling. To realize this potential, the design of the SESAM needs to be adjusted to support higher pulse energies. The devices presented here use semiconductor layers on top of the absorbers to reduce the fluence in the quantum wells. Further increasing the number of semiconductor layers would lead to a prohibitively strong inverse saturable absorption, limiting pulse energy. Thus, we plan to replace the semiconductor layers with a dielectric top-coating (DTC) [36]. Since using a DTC implies a change in the top-most material, the bond and/or DTC design will have to be adapted to maintain a high bond quality.

## 5. Conclusions

We demonstrate a new method to fabricate high-power compatible SESAMs with an adjustable thermal lens by bonding sapphire to the front side. We use the fabricated SESAMs to mode-lock a high-power TDL and reach 233 W of average power. We attribute the improvement of 70 W compared to a standard SESAM in the same cavity to the compensation of the thermal lenses inside the cavity. The strength of the thermal lens can be adjusted by changing the thickness of the sapphire. This control enables optimization of SESAM for different cavities, and the creation of an “athermal” SESAM with no overall thermal lensing. Another possibility is to use a strongly wedged sapphire window to allow continuous tuning of the sapphire thickness on a

single sample. We discuss potential further improvements to the SESAMs to reach even higher powers such as including a dielectric top-coating. The bonding method is highly flexible and can be performed at room temperature, making it applicable to a wide range of materials and devices. The resulting bond is well-suited for intra-cavity components in high peak-intensity applications. One potential future application is the creation of high-power or monolithic Vertical External Cavity Semiconductor Lasers (VECSELs).

**Funding.** Science and Technology Facilities Council (ST/N005422/1, ST/V001736/1); Schweizerischer Nationalfonds zur Förderung der Wissenschaftlichen Forschung (200020\_172644).

**Acknowledgments.** The ETH Zurich authors would like to thank Prof. Martin M. Fejer for helpful discussions in the early stages of the project. Additionally, we would like to thank Alexander Nussbaum-Lapping and Marco Gaulke for help with some of the characterization measurements. We also thank Dr. Valentin Wittwer, Dr. Olga Razskazovskaya, and Prof. Dr. Thomas Südmeyer (University of Neuchatel) for coating the sapphire windows and providing some of the dispersive mirrors. The University of Glasgow authors would like to acknowledge our colleagues in the Institute of Gravitational Research, LIGO Scientific Collaboration, the GEO600 project and the Scottish Universities Physics Alliance for their interest in the work. The authors would like to thank the University of Glasgow and the Science and Technology Facilities Council for their financial support.

**Disclosures.** The ETH Zurich authors signed an NDA with TRUMPF with regards to the thin-disk module and head.

**Data availability.** Data underlying the results presented in this paper are not publicly available at this time but may be obtained from the authors upon reasonable request.

## References

1. F. Saltarelli, I. J. Graumann, L. Lang, D. Bauer, C. R. Phillips, and U. Keller, "Power scaling of ultrafast oscillators: 350-W average-power sub-picosecond thin-disk laser," *Opt. Express* **27**(22), 31465–31474 (2019).
2. M. Müller, C. Aleshire, A. Klenke, E. Haddad, F. Légaré, A. Tünnermann, and J. Limpert, "10.4 kW coherently combined ultrafast fiber laser," *Opt. Lett.* **45**(11), 3083–3086 (2020).
3. P. Russbuehdt, T. Mans, J. Weitenberg, H. D. Hoffmann, and R. Poprawe, "Compact diode-pumped 1.1 kW Yb:YAG Innoslab femtosecond amplifier," *Opt. Lett.* **35**(24), 4169–4171 (2010).
4. J.-P. Negel, A. Loescher, A. Voss, D. Bauer, D. Sutter, A. Killi, M. A. Ahmed, and T. Graf, "Ultrafast thin-disk multipass laser amplifier delivering 1.4 kW (4.7 mJ, 1030 nm) average power converted to 820 W at 515 nm and 234 W at 343 nm," *Opt. Express* **23**(16), 21064–21077 (2015).
5. U. Keller, K. J. Weingarten, F. X. Kärtner, D. Kopf, B. Braun, I. D. Jung, R. Fluck, C. Hönninger, N. Matuschek, and J. Aus der Au, "Semiconductor saturable absorber mirrors (SESAMs) for femtosecond to nanosecond pulse generation in solid-state lasers," *IEEE J. Sel. Top. Quantum Electron.* **2**(3), 435–453 (1996).
6. J. Brons, V. Pervak, E. Fedulova, D. Bauer, D. Sutter, V. Kalashnikov, A. Apolonskiy, O. Pronin, and F. Krausz, "Energy scaling of Kerr-lens mode-locked thin-disk oscillators," *Opt. Lett.* **39**(22), 6442–6445 (2014).
7. C. J. Saraceno, F. Emaury, C. Schriber, A. Diebold, M. Hoffmann, M. Golling, T. Südmeyer, and U. Keller, "Toward Millijoule-Level High-Power Ultrafast Thin-Disk Oscillators," *IEEE J. Select. Topics Quantum Electron.* **21**(1), 106–123 (2015).
8. S. Piehler, T. Dietrich, P. Wittmüss, O. Sawodny, M. A. Ahmed, and T. Graf, "Deformable mirrors for intra-cavity use in high-power thin-disk lasers," *Opt. Express* **25**(4), 4254–4267 (2017).
9. A. Diebold, T. Zengerle, C. G. E. Alfieri, C. Schriber, F. Emaury, M. Mangold, M. Hoffmann, C. J. Saraceno, M. Golling, D. Follman, G. D. Cole, M. Aspelmeyer, T. Südmeyer, and U. Keller, "Optimized SESAMs for kilowatt-level ultrafast lasers," *Opt. Express* **24**(10), 10512–10526 (2016).
10. I. J. Graumann, F. Saltarelli, L. Lang, V. J. Wittwer, T. Südmeyer, C. R. Phillips, and U. Keller, "Power-scaling of nonlinear-mirror modelocked thin-disk lasers," *Opt. Express* **27**(26), 37349–37363 (2019).
11. F. Saltarelli, A. Diebold, I. J. Graumann, C. R. Phillips, and U. Keller, "Modelocking of a thin-disk laser with the frequency-doubling nonlinear-mirror technique," *Opt. Express* **25**(19), 23254–23266 (2017).
12. D.-H. Gwo, *Two unique aspects of gravity probe-B star-tracking space telescope: (1) focal-plane roof-edge diffraction and (2) fused-quartz bonding for 2.5-Kelvin applications* (SPIE, 1998).
13. R. Douglas, A. A. V. Veggel, L. Cunningham, K. Haughian, J. Hough, and S. Rowan, "Cryogenic and room temperature strength of sapphire jointed by hydroxide-catalysis bonding," *Class. Quantum Grav.* **31**(4), 045001 (2014).
14. S. Sinha, K. E. Urbanek, A. Krzywicki, and R. L. Byer, "Investigation of the suitability of silicate bonding for facet termination in active fiber devices," *Opt. Express* **15**(20), 13003–13022 (2007).
15. A.-M. A. van Veggel and C. J. Killow, "Hydroxide catalysis bonding for astronomical instruments," *Adv. Opt. Technol.* **3**(3), 293–307 (2014).
16. B. P. Abbott, R. Abbott, T. Abbott, M. Abernathy, F. Acernese, K. Ackley, C. Adams, T. Adams, P. Addesso, and R. Adhikari, "Observation of gravitational waves from a binary black hole merger," *Phys. Rev. Lett.* **116**(6), 061102 (2016).

17. V. Mangano, A. A. van Veggel, R. Douglas, J. Faller, A. Grant, J. Hough, and S. Rowan, "Determination of the refractive index and thickness of a hydroxide-catalysis bond between fused silica from reflectivity measurements," *Opt. Express* **25**(4), 3196 (2017).
18. G. Lacaille, V. Mangano, A.-M. A. van Veggel, C. J. Killow, P. E. MacKay, S. Rowan, and J. Hough, "Optical characterisation of hydroxide catalysed bonds applied to phosphate glass," in *Optifab 2017* (International Society for Optics and Photonics 2017), p. 1044825.
19. G. T. Nick and R. C. Neil, "Improved bond strength characterization of chemically activated direct bonding (CADB) epoxy-free bonded solid state laser materials," in *Proc.SPIE*(2010).
20. M. De Vido, D. Meissner, S. Meissner, K. Ertel, P. J. Phillips, P. D. Mason, S. Banerjee, T. J. Butcher, J. M. Smith, and C. Edwards, "Characterisation of adhesive-free bonded crystalline Yb: YAG for high energy laser applications," *Opt. Mater. Express* **7**(2), 425–432 (2017).
21. K. S. Prabhu, T. L. Schmitz, P. G. Ifju, and J. G. Daly, "A survey of technical literature on adhesive applications for optics," in *New Developments in Optomechanics* (International Society for Optics and Photonics 2007), p. 666507.
22. C. Y. Sheng, "Effects of laser-induced damage on optical windows in the presence of adhesives under simulated thermal-vacuum conditions," in *Laser-Induced Damage in Optical Materials: 2006* (International Society for Optics and Photonics 2007), p. 64030H.
23. K. Fujioka, A. Sugiyama, Y. Fujimoto, J. Kawanaka, and N. Miyanaga, "Ion diffusion at the bonding interface of undoped YAG/Yb: YAG composite ceramics," *Opt. Mater.* **46**, 542–547 (2015).
24. I. Mukhin, E. Perevezentsev, and O. Palashov, "Fabrication of composite laser elements by a new thermal diffusion bonding method," *Opt. Mater. Express* **4**(2), 266–271 (2014).
25. A. Berthold, L. Nicola, P. Sarro, and M. Vellekoop, "Glass-to-glass anodic bonding with standard IC technology thin films as intermediate layers," *Sens. Actuators, A* **82**(1-3), 224–228 (2000).
26. C. J. Killow, E. D. Fitzsimons, J. Hough, M. Perreur-Lloyd, D. I. Robertson, S. Rowan, and H. Ward, "Construction of rugged, ultrastable optical assemblies with optical component alignment at the few microradian level," *Appl. Opt.* **52**(2), 177–181 (2013).
27. D. -H. Gwo, "*Hydroxide-catalyzed Bonding*," (The Board of Trustees of the Leland Stanford Junior University (Stanford, CA), 2003).
28. Y.-L. Sun, Y.-X. Ye, X.-H. Shi, Z.-Y. Wang, C.-J. Yan, L.-L. He, Z.-H. Lu, and J. Zhang, "A hybrid silicon-sapphire cryogenic Fabry–Perot cavity using hydroxide catalysis bonding," *Class. Quantum Grav.* **36**(10), 105007 (2019).
29. D. -H. Gwo, "*Ultra precision and reliable bonding method*," (The Board of Trustees of the Leland Stanford Junior University (Stanford, CA), 2001).
30. J. R. Vig, "UV/ozone cleaning of surfaces," *Journal of Vacuum Science & Technology A: Vacuum*, *J. Vac. Sci. Technol., A* **3**(3), 1027–1034 (1985).
31. P. Zhang, M. Jiang, R. Zhue, D. Zhang, and Y. Song, "Thermal conductivity of GaAs/AlAs distributed Bragg reflectors in semiconductor disk laser: comparison of molecular dynamics simulation and analytic methods," *Appl. Opt.* **56**(15), 4537 (2017).
32. J. Neuhaus, J. Kleinbauer, A. Killi, S. Weiler, D. Sutter, and T. Dekorsy, "Passively mode-locked Yb:YAG thin-disk laser with pulse energies exceeding 13  $\mu$ J by use of an active multipass geometry," *Opt. Lett.* **33**(7), 726 (2008).
33. F. X. Kartner, I. D. Jung, and U. Keller, "Soliton mode-locking with saturable absorbers," *IEEE J. Sel. Top. Quan. Electron.* **2**(3), 540–556 (1996).
34. A. Diebold, F. Saltarelli, I. J. Graumann, C. J. Saraceno, C. R. Phillips, and U. Keller, "Gas-lens effect in kW-class thin-disk lasers," *Opt. Express* **26**(10), 12648–12659 (2018).
35. F. Saltarelli, D. Koenen, L. Lang, I. J. Graumann, C. R. Phillips, and U. Keller, "Beam quality in high-power thin-disk lasers: influence and measurement of the radial inversion profile," in *Laser Congress 2019 (ASSL, LAC, LS&C)* (Optical Society of America, Vienna, 2019), p. JM5A.35.
36. C. J. Saraceno, C. Schriber, M. Mangold, M. Hoffmann, O. H. Heckl, C. R. E. Baer, M. Golling, T. Südmeyer, and U. Keller, "SESAMs for high-power oscillators: design guidelines and damage thresholds," *IEEE J. Sel. Top. Quan. Electron.* **18**(1), 29–41 (2012).